NREL
NATIONAL RENEWABLE ENERGY LABORATORY

Three-Dimensional Numerical Evaluation of Thermal Performance of Uninsulated Wall Assemblies

Preprint

El Hassan Ridouane and Marcus V. A. Bianchi

Presented at the ASME 2011 International Mechanical Engineering Congress and Exposition
Denver, Colorado
November 11-17, 2011

Conference Paper
NREL/CP-5500-52389
November 2011

Contract No. DE-AC36-08GO28308

NOTICE

Available electronically at http://www.osti.gov/bridge

Available for a processing fee to U.S. Department of Energy
and its contractors, in paper, from:

U.S. Department of Energy
Office of Scientific and Technical Information

P.O. Box 62
Oak Ridge, TN 37831-0062
phone: 865.576.8401
fax: 865.576.5728
email: mailto:reports@adonis.osti.gov

Available for sale to the public, in paper, from:

U.S. Department of Commerce
National Technical Information Service
5285 Port Royal Road
Springfield, VA 22161
phone: 800.553.6847
fax: 703.605.6900
email: orders@ntis.fedworld.gov
online ordering: http://www.ntis.gov/help/ordermethods.aspx

Cover Photos: (left to right) PIX 16416, PIX 17423, PIX 16560, PIX 17613, PIX 17436, PIX 17721

Printed on paper containing at least 50% wastepaper, including 10% post consumer waste.

THREE-DIMENSIONAL NUMERICAL EVALUATION OF THERMAL PERFORMANCE OF UNINSULATED WALL ASSEMBLIES

El Hassan Ridouane, PhD
National Renewable Energy Laboratory
1617 Cole Blvd
Golden, Colorado, USA
Email: elhassan.ridouane@nrel.gov

Marcus V.A. Bianchi, PhD
National Renewable Energy Laboratory
1617 Cole Blvd
Golden, Colorado, USA
Email: marcus.bianchi@nrel.gov

ABSTRACT

Uninsulated wall assemblies are typical in older homes, as many were built before building codes required insulation. Building engineers need to understand the thermal performance of these assemblies as they consider home energy upgrades if they are to properly predict pre-upgrade performance and, consequently, prospective energy savings from the upgrade. Most whole-building energy simulation tools currently use simplified, 1D characterizations of building envelopes and assume a fixed thermal resistance that does not vary over a building's temperature range.

This study describes a detailed 3D computational fluid dynamics model that evaluates the thermal performance of uninsulated wall assemblies. It accounts for conduction through framing, convection, and radiation and allows for material property variations with temperature. Parameters that were varied include ambient outdoor temperature and cavity surface emissivity. The results may serve as input for building energy simulation tools that model the temperature-dependent energy performance of homes with uninsulated walls.

INTRODUCTION

The global interest in energy conservation through improved building enclosures has driven a steady stream of fundamental and applied studies that focus on reducing thermal loads and maintaining occupant comfort. Accurate estimates of heat transfer through building assemblies, accompanied by low-cost energy upgrades, support efforts to reduce energy consumption in older homes. This study evaluates the thermal performance of uninsulated walls in low-rise, wood-framed homes. Combined heat transfer by natural convection and radiation inside wall cavities is an important mechanism in the total heat exchange through these walls.

Numerous studies address natural convection flows in 2D cavities of square and rectangular cross sections. Early work was reviewed by Bejan [1], Jaluria [2], and Raithby and Hollands [3]. These studies concentrated on pure natural convection with various thermal boundary conditions (Douamna et al. [4], Fusegi et al. [5], and Lakhal et al. [6], and on different aspect ratios and angles of inclination (Rahman and Sharif [7]). Experimental studies reported by Catton [8] provided insight into the complexity of the problem. The interaction between natural convection and thermal radiation was the subject of numerical studies by Akiyama and Chong [9], Pak and Park [10], Ridouane et al. [11], and Yucel et al. [12]. Their results showed that surface radiation significantly alters temperature distribution and flow patterns.

Park et al. [13] focused on building enclosures and performed numerical simulations to investigate the heat transfer through a standard residential uninsulated stud wall structure. Indoor and outdoor air temperatures were fixed at 294 K (70°F) and 300 K (80°F), respectively. The authors considered five test cases, with different approximations, to address the coupled heat transfer by convection and radiation. The results showed that thermal radiation is an important transport mechanism in uninsulated walls, even with modest temperature differences: adding a reflective layer (foil liner) on one inner surface of the cavity reduced the heat transfer by 50%. Calculated heat transfer rates through the wall were within 3% of the values published in the 1977 ASHRAE Handbook of Fundamentals. ASHRAE [14] provides a table listing thermal resistance values for enclosed air spaces under various conditions, depending on cavity surface emissivity. These values are for well-sealed cavities and selected combinations of mean temperatures and temperature differences, but do not represent a building's operating conditions. For uninsulated 2 × 4 walls, the table shows slight variations in cavity resistance with the mean temperature and temperature difference.

Barbour et al. [15] used a calibrated hot box to test a number of wall assemblies, to provide measured thermal resistance for commonly used steel-framed wall configurations.

They found that insulating sheathing significantly decreases the effects of thermal bridging and that the ASHRAE Zone Method overestimates thermal performance of metal stud walls with uninsulated cavities by up to 15%. Lorente [16] studied heat loss through building walls with closed, open, and deformable cavities, which appear in double-pane windows that have moderate pressure differences between the inner and outer panes. Heat losses are largely due to convective heat transfer inside vertical wall cavities.

Aviram et al. [17] used a guarded hot box to experimentally investigate the heat transfer through a variable aspect ratio cavity. A block and brick wall cavity measuring 1.2 × 1.2 m^2 (3.94 × 3.94 ft^2) was tested at cavity depths of 78, 60, and 40 mm (3.1 in., 2.4 in., and 1.6 in.). Results showed that circulation intensity decreased and thermal resistance increased with increased aspect ratio. The resistance of the cavity increased by 66% when the cavity depth decreased from 78 mm (3.1 in.) to 40 mm (1.6 in.). Similar numerical studies were conducted by Manz [18] and Xaman et al. [19] in rectangular cavities with aspect ratios 20, 40, and 80 (typical aspect ratios in wall cavities is 27.4 for 2 × 4 construction and 17.5 for 2 × 6 construction). Antar and Baig [20] studied conjugate heat transfer by conduction and convection in a hollow block and showed that increasing the number of cavities while keeping the block width constant significantly increased thermal resistance.

The objective of the present study is to evaluate the thermal performance of uninsulated walls by solving the 3D combined heat transfer by conduction, convection, and radiation in the wall assembly, including the framing elements. The model can be applied over a wide range of operating conditions. The results are compared to the output of a 2D model [21], which was modified to model variable thermophysical properties, and to the current input of whole-building energy simulation tools (fixed thermal resistance evaluated at 297 K (75˚F) mean temperature).

NUMERICAL MODEL

Figure 1 presents the geometric configuration, which is a 0.41-m (16-in.) × 0.14-m (5.5-in.) × 2.44-m (8-ft) section of a standard 0.05 × 0.1 m^2 (2 × 4 $in.^2$) residential stud wall. Starting from the inside (left), the wall consists of a 0.0127-m (0.5-in.) gypsum wallboard, a 0.089-m (3.5-in.) air cavity limited by 2 × 4 studs, a 0.0127-m (0.5-in.) layer of sheathing, and a 0.025-m (1-in.) layer of wood siding that is exposed to outside air. The distance between the studs is 0.41-m (16-in.) centers. The cavity is closed at top and bottom by adiabatic sills. We took advantage of the periodicity and modeled only a section of the wall that contains one air cavity and half of each limiting stud. The thermophysical properties of air, wood studs, wood siding, and sheathing were allowed to vary with temperature. Air properties varied as piecewise-linear functions of temperature, except density, which follows the ideal gas law. An air property $\Phi(T)$ at a temperature T is determined through this equation:

$$\Phi(T) = \Phi_n + \frac{\Phi_{n+1}-\Phi_n}{T_{n+1}-T_n}(T - T_n) \qquad (1)$$

where (T_n, Φ_n) are data pairs entered manually into the model. Density of wood products was considered independent of temperature. The thermal conductivity of dry wood (studs, siding, and sheathing) was obtained from the Wood Handbook [22]: as the temperature increases, the thermal conductivity increases 3% per 10 K. Due to lack of information, the gypsum properties were assumed to be constant. As a reference point, Tables 1 and 2 list the material properties of different layers of the wall assembly evaluated at 297 K (75˚F) [14].

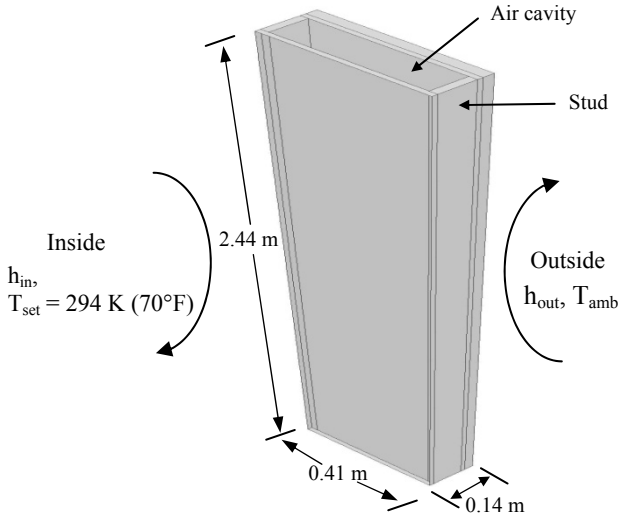

Figure 1 *Schematic of the wall structure, which consists of a 0.41-m (16-in.) long × 0.14-m (5.5-in.) wide × 2.44-m (8-ft) high section of a standard 2 × 4 residential stud wall.*

Table 1. Properties of Building Materials Used in This Study Evaluated at 297 K – SI units

Material	Density kg/m^3	Conductivity W/m·K	Specific Heat J/kg·K
Gypsum board	641	0.158	1130
Sheathing	288	0.055	1298
Wood siding	689	0.182	1172
Wood stud	689	0.182	1172

Table 2. Properties of Building Materials Used in This Study Evaluated at 75˚F – English units

Material	Density lb/ft^3	Conductivity Btu/h·ft·°F	Specific Heat Btu/lb·°F
Gypsum board	40	0.0916	0.27
Sheathing	18	0.0316	0.31
Wood siding	43	0.1054	0.28
Wood stud	43	0.1054	0.28

The operating conditions considered resulted in high values of the Rayleigh number (~ 10^9 and higher), so the

airflow is assumed to be turbulent. Under steady-state conditions, the governing equations are the heat conduction equation in the solid parts of the wall and 3D Navier-Stokes and energy equations in the air. We used the surface-to-surface method described by Modest [23] to calculate the radiative exchange between the inner surfaces of the wall cavity. Two surface emissivities of 0.05 and 0.8 were considered and all participating surfaces were assumed to be gray and diffuse. The emissivity of 0.8 represents common building materials and emissivity of 0.05 corresponds to a highly reflective aluminum foil surface when a reflective insulation (radiant barrier) is added to reduce radiation transfer. The model assumes a tight wall and ignores infiltration and exfiltration.

We used the finite volume method of the commercial software FLUENT 6.3 [24] to numerically solve the governing equations. Turbulence is modeled by the standard k–ε model. An implicit segregated solver is employed and all discretization schemes are of second-order accuracy or higher. The QUICK scheme is used for momentum, energy, and density discretization. A second-order scheme is applied in the pressure discretization and the SIMPLE scheme is used in pressure-velocity coupling. We assessed simulation convergence by monitoring computed conservation equations residuals and converging surface monitors. The absolute convergence criteria for velocity, temperature, and heat flux monitors, at select locations in the domain, were set to 10^{-6}. We conducted a formal grid sensitivity study to ensure the numerical results were independent of grid resolution. We examined grid sizes ranging from 150,000 to 350,000 hexahedral elements at the highest ΔT used (61 K [110°F]). Grid independence was within 1% with the nonuniform grid size of 259,200 hexahedral elements.

Verification of the numerical model was done in a previous study (Ridouane and Bianchi [21]) by comparing the results of a 2D model with those published 2009 ASHRAE Fundamentals [14] and in Park et al. [13]. Both comparisons showed good agreement.

RESULTS AND DISCUSSION

The 3D numerical model was used to simulate the performance of uninsulated wall assemblies typical in older wood frame homes. A parametric study was performed varying the ambient outdoor temperature from 233 K (-40˚F) to 311 K (100˚F) and using two surface emissivities of 0.05 and 0.8. The indoor temperature was maintained at 294 K (70°F). The convective heat transfer coefficients at the indoor and outdoor surfaces were assumed to be 8.33 $W/m^2 \cdot K$ (1.47 $Btu/hr ft^{2,\circ}F$) and 33.33 $W/m^2 \cdot K$ (5.88 $Btu/hr ft^{2,\circ}F$), respectively. Local and average quantities are provided for different operating conditions. The output of the 3D model is compared to the results of a 2D model to verify the need for the additional dimension to accurately predict the thermal characteristics of uninsulated wall assemblies. The effects of surface emissivity and ambient temperature on temperature distribution, thermal resistance, and heat flux through the wall are presented and discussed.

Local Quantities

Figure 2 illustrates the temperature distribution at two typical cross sections of the wall for winter conditions when the ambient temperature was 255 K (0°F). Cross section A is the vertical midplane perpendicular to the wall; cross section B is the vertical midplane parallel to the wall. Both divide the air cavity in half. The dimensions in the temperature plots are not to scale, to allow visualization of the flow patterns in the entire domain. Building materials, other than metals, have a high thermal emissivity around 0.8. For illustration purposes, we also simulated the case of foil faced materials (reflective insulation) having an emissivity of 0.05. At this high temperature difference between the indoors and outdoors (ΔT), strong clockwise flow circulation was formed in the cavity with high temperature gradients near the hot (left) and cold (right) vertical boundaries. The temperature distribution associated with this circulation is clearly seen in cross section A; cross section B provides the temperature gradients along the depth of the wall and shows the effects of the studs on airflow at both ends of the wall section. This effect is not accounted for in 1D and 2D models. Changes in the scale of the color bar between ε = 0.05 and ε = 0.8 plots show how significant the effect of surface emissivity is on temperature distribution. Except for the change in flow direction, similar trends were observed for summer conditions when the ambient temperature was 311 K (100°F) (Figure 3). Also, the indoor/outdoor temperature difference in Figure 3 is much smaller than that in Figure 2.

Convection boundary conditions imposed at the internal and external surfaces of the wall assembly allow the surface temperatures to vary in space. This variation is depicted in Figure 4 along the vertical symmetry line of the internal and external surfaces of the wall for 255 K (0°F) and 311 K (100°F) ambient temperatures. A 3.6 K (6.5°F) difference was found between the top and the bottom of the internal surface at an ambient temperature of 255 K (0°F). This difference is a function of the temperature difference and the overall thermal resistances.

Figure 5 presents the variations of the local heat flux, q, along the vertical symmetry line of the internal and external surfaces of the wall with an emissivity of 0.8 when the ambient temperature is 255 K (0°F). For this ΔT there was a clockwise airflow circulation in the cavity (see Figure 2(b)). Starting with the inside surface (dashed curve), the heat flux is high at the floor level where the cold air first hits the hot surface and decreased as the height increased. The opposite occurred on the outside surface with the hot air hitting the cold surface at the top resulting in a high value of q, which decreased as the height decreased toward the floor.

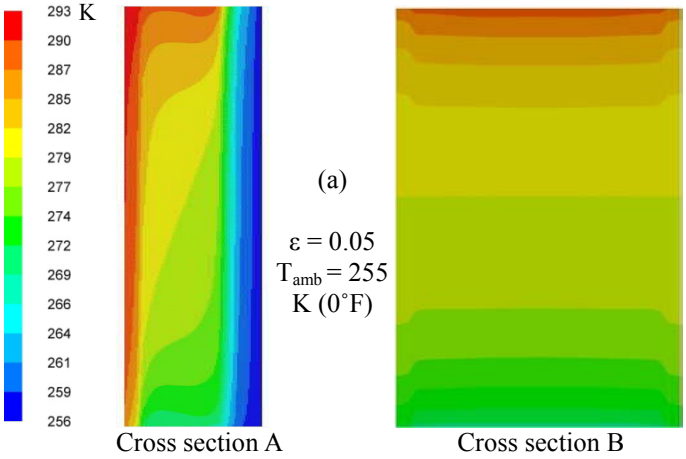

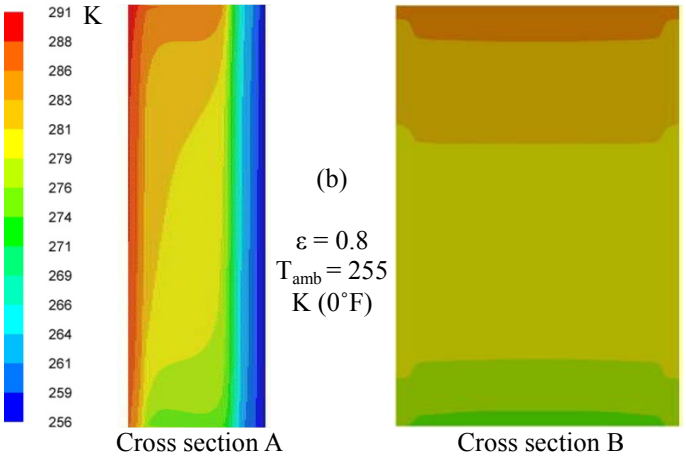

Figure 2 *Effect of surface emissivity, ε, on the temperature distribution in the wall when the outdoor ambient temperature is 255 K (0°F).*

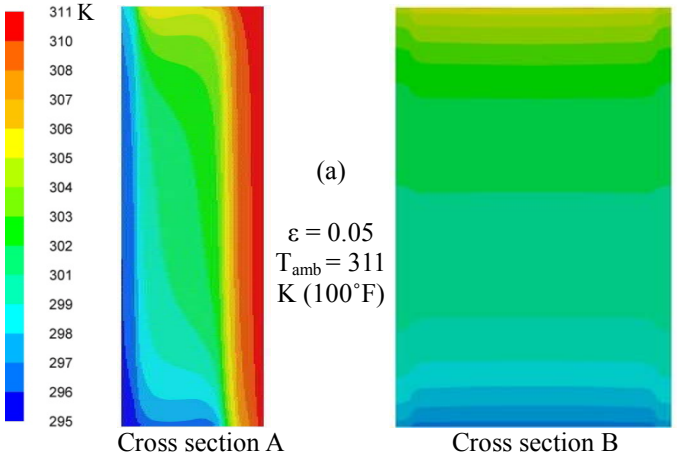

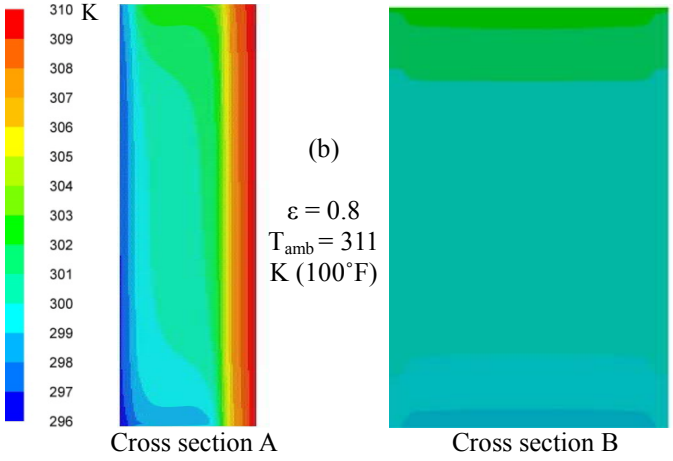

Figure 3 *Effect of surface emissivity, ε, on the temperature distribution in the wall when the outdoor ambient temperature is 311 K (100°F).*

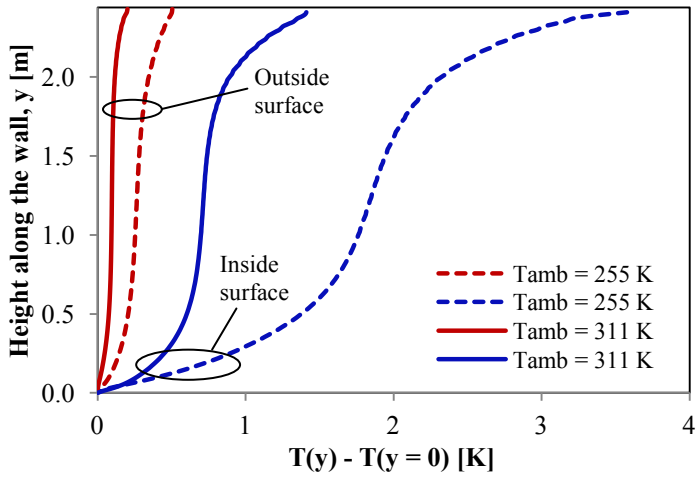

Figure 4 *Temperature profile along the vertical symmetry line of the internal and external surfaces of the wall. The graph shows changes in temperature relative to the bottom of the wall with an emissivity, ε, of 0.8.*

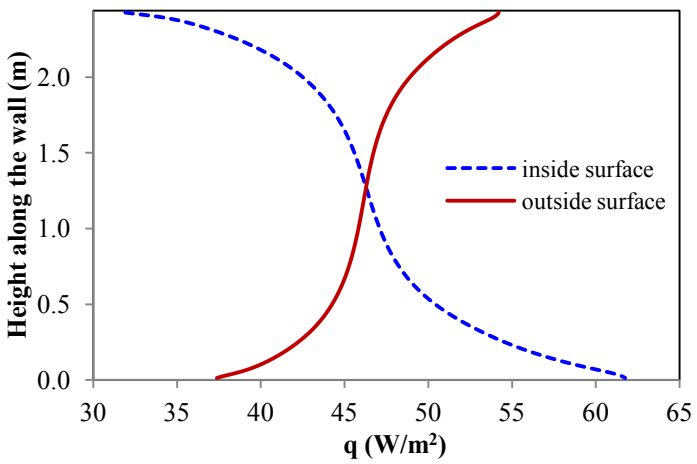

Figure 5 *Local heat flux along the vertical symmetry line of the internal and external surfaces of the wall with an emissivity, ε, of 0.8 when the ambient temperature is 255 K (0°F).*

Average Quantities

The total resistance, R_{tot}, of the wall assembly, including that of framing, air cavity, and inside and outside films, is shown in Figure 6 as a function of the ambient temperature and surface emissivity. The output of the 2D model, which also accounts for the effect of variable material properties, includes the resistance of the studs in parallel with the air cavity resistance. When the emissivity is equal to 0.8, the resistance predicted by both 2D and 3D models is high at 233 K (-40°F) and decreases with the ambient temperature to reach a minimum around 283 K (50˚F) for ambient temperatures below the interior temperatures. R_{tot} decreases quickly at higher ambient temperatures. Good agreement is observed between the 2D and 3D predictions; differences are within 1%. The horizontal dashed line indicates the resistance used in the traditional approach, which is evaluated at 297 K (75˚F). When the emissivity is lowered to 0.05 (Figure 6(b)), the minimum does not take place in the range investigated and the thermal resistance is characterized by a monotonic increase between 233 K (-40°F) and 294 K (69°F). For heating conditions the maximum deviation between 2D and 3D model predictions is 4%. When the ambient temperature is higher than the exterior temperature, the thermal resistance predicted by the 2D model can be up to 14% higher. However, larger differences are found at temperature differences below 5.4 K (10°F), where the heat transfer rate is small.

The effect of allowing the thermophysical properties of air and wood to vary with the local temperature is illustrated in Figure 7, where the total resistance is shown as a function of the ambient temperature. The 3D model was used to predict the total resistance of the assembly for constant[1] and variable material properties. The assumption of constant thermophysical properties, evaluated at 297 K (75˚F), underpredicted the wall performance when the ambient temperature was below the set point of 294 K (70˚F): the lower the ambient temperature, the greater the difference is, reaching 8% at 232 K (-40°F). Good agreement is observed around T_{amb} of 297 K (75˚F) where the constant properties were evaluated. Opposite trends occurred at ambient temperatures higher than 300 K (80°F): constant properties predicted higher resistances for the wall, but the temperature differences are smaller, so the discrepancy is smaller (2% at 311 K).

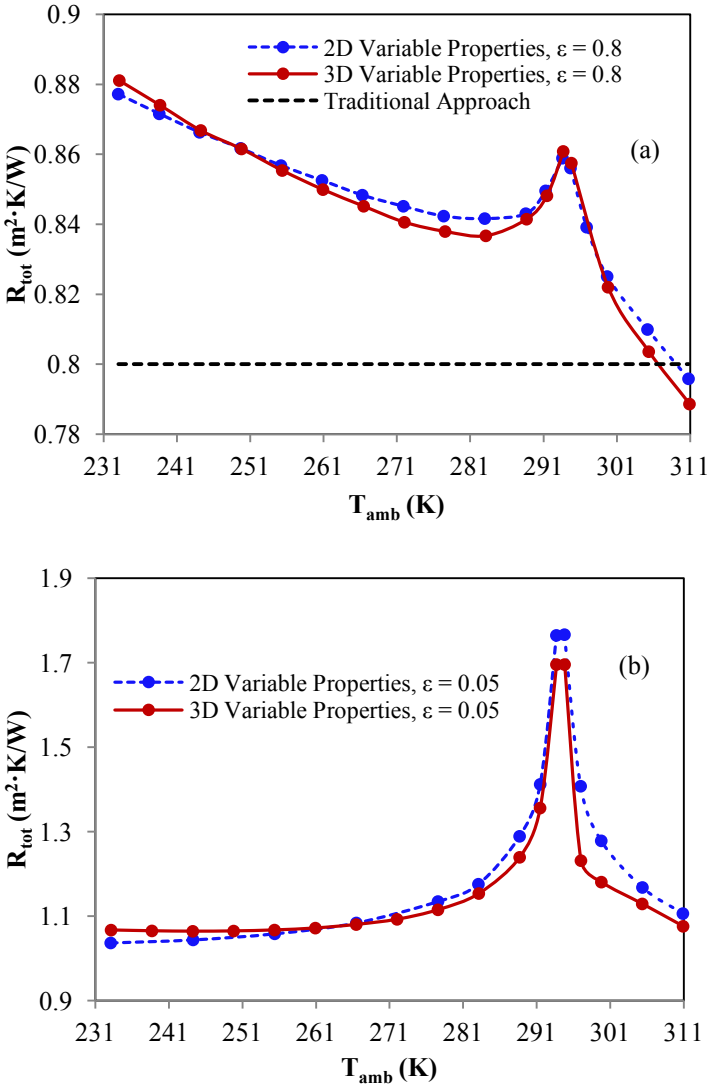

Figure 6 *Thermal resistance of the wall assembly, predicted using 2D and 3D models, as a function of the outdoor ambient temperature. (a) High surface emissivity of 0.8 and (b) low surface emissivity of 0.05.*

Further simulations were performed separating the effects of variable properties of air and wood to evaluate the relative importance of each of them. When only the thermophysical properties of air were allowed to vary, no effect on the thermal resistance was observed. The difference shown in Figure 7 is

[1] All properties are fixed, except air density, which followed the ideal gas law.

due solely to the effect of variable thermophysical properties of wood: at lower temperatures, the thermal conductivity is smaller, leading to an increase in the thermal resistance of the assembly due to the sheathing and siding higher resistance.

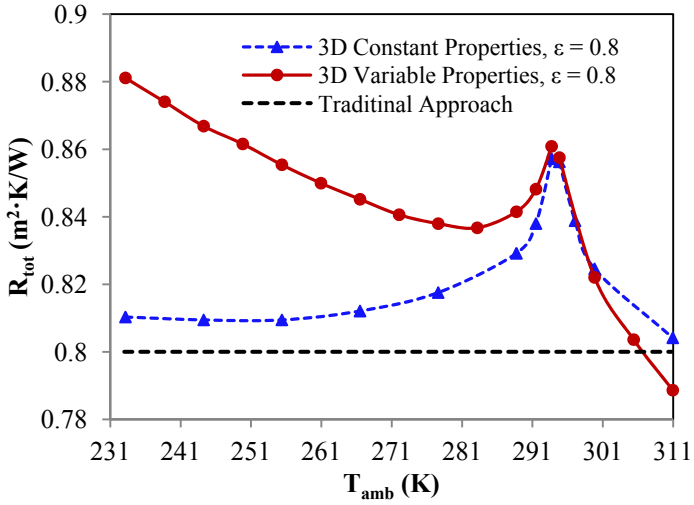

Figure 7 *Effect of temperature-dependent material properties on thermal resistance of the wall assembly for 0.8 surface emissivity.*

To understand the impact of the studs on the heat transfer through the assembly, we examined the distribution of the local heat flux at midheight of the wall. A low ambient temperature of 233 K (-40°F) was selected (see Figure 8(a)). This distribution is slightly affected by the studs; their effect has reduced the heat extracted by the air circulation from solid surfaces because of lower air velocities in these regions. The order of magnitude of this reduction is quantified in Figure 8(b) by the variation of q on line 1 at the interface between wallboard and air cavity. The heat flux in 3D was equal to that of 2D in the middle of the cavity and decreased toward the studs. Lower values of q translate into higher resistances.

A detailed 3D model is implemented to contrast the thermal performance of the uninsulated wall assembly with the predictions of the 2D model and with the traditional approach that assumes constant R_{tot}. The latter, which evaluates R_{tot} at 297 K (75˚F) mean temperature, is currently used in many whole-building energy simulation tools.

Figure 9(a) compares predictions of the thermal performance of the wall assembly using 2D and 3D models when the surface emissivity is 0.8. The comparison was done in terms of the total heat flux through the wall as a function of the ambient temperature. The heat flux decreases with the ambient temperature, and crosses the x-axis at the indoor set temperature of 294 K (70˚F). The 2D model predicted comparable heat fluxes to those of 3D model for winter and summer conditions. The traditional approach, however, predicted slightly higher heat fluxes for winter conditions and lower heat fluxes for summer conditions when the outdoor temperature is higher than 300 K (80˚F) (Figure 9 (b)).

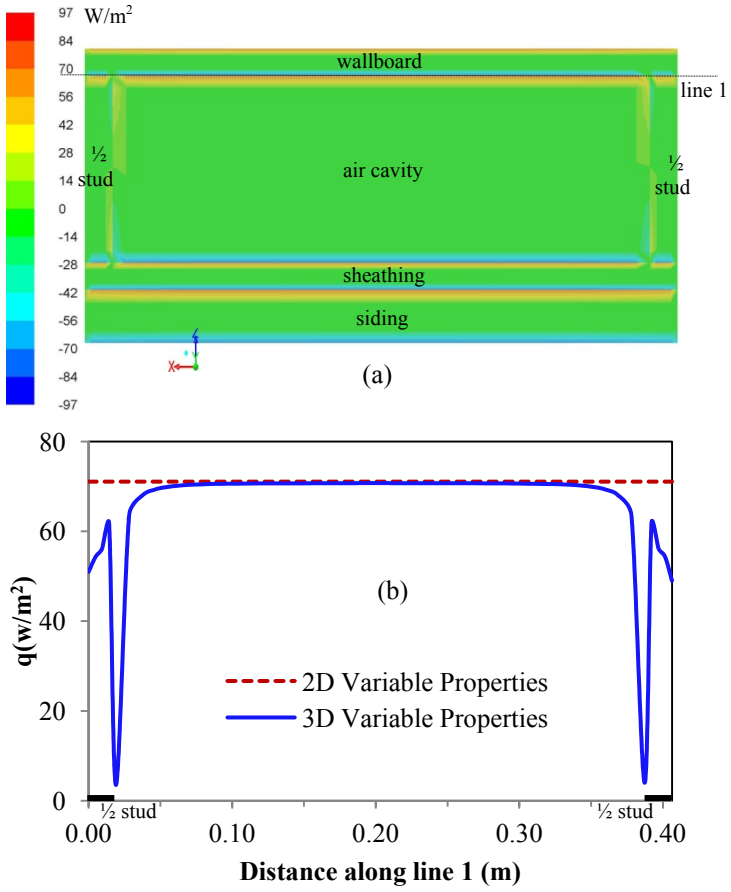

Figure 8 *Heat flux at ambient temperature of 233 K (-40°F) and emissivity of 0.8. (a) Distribution on the horizontal symmetry plane of the wall. (b) Profile on line 1 from right to left.*

Table 5 summarizes the output of the different approaches and lists the relative differences between each model prediction and those of the 3D model. Significant differences between the 3D and the traditional approach were obtained, which ranged from 11.4% at 291 K (65˚F)[2] to -2.4% at 311 K (100˚F). Of particular interest are the differences at lower ambient temperatures, where they can be as high as 9.3% on very cold days; both the 2D and 3D models predict lower heat transfer rates through the wall compared to the traditional approach. Smaller differences were found when comparing the 3D and 2D model results, with the highest difference of -3.1% at 300 K (80˚F)[3]. If these results are implemented into building energy simulation tools, they would reduce the predicted heating load. For summer conditions the 3D model predicted slightly higher cooling loads for T_{amb} higher than 300 K (80˚F).

[2] Differences that take place near a zero temperature difference may be interesting for model testing, but not for their effect on heating and cooling load predictions.

[3] See previous footnote.

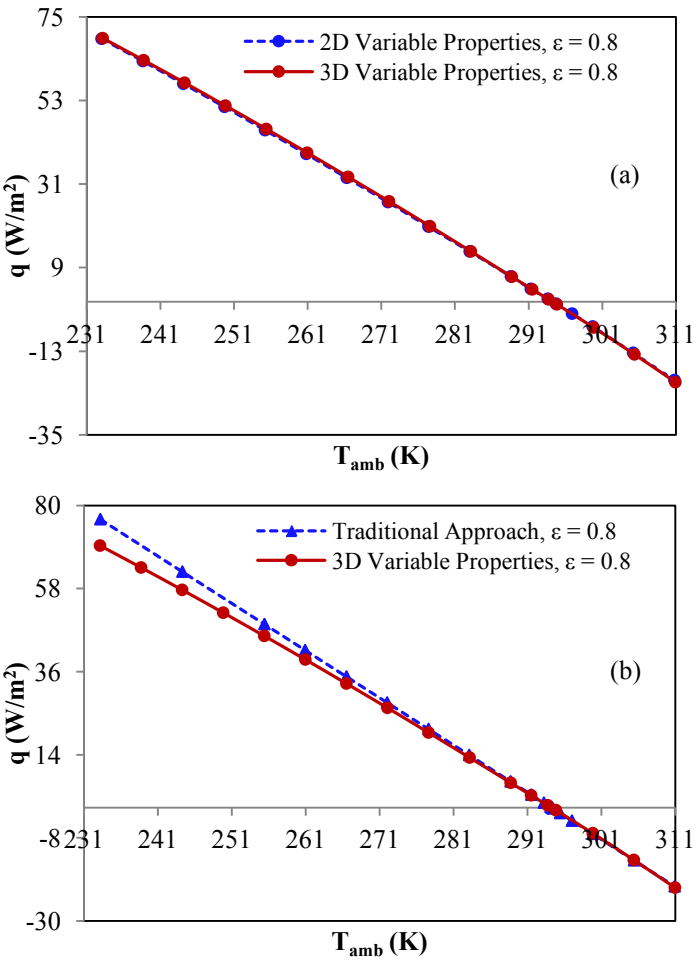

Figure 9 *Total heat flux through the wall assembly as a function of T_{amb} when the surface emissivity is 0.8. (a) comparison of 3D with 2D and (b) comparison of 3D with the traditional approach, assuming constant resistance evaluated at 297 K (75˚F) mean temperature.*

Table 5. Comparison of the Total Heat Flux Through the Wall Assembly (ε = 0.8)

T_{amb} K	Traditional Approach W/m²	2D W/m²	3D W/m²	% Diff 3D/Traditional Approach	% Diff 3D/2D
233	76.4	70.2	69.3	9.3	1.3
255	48.6	45.1	45.4	6.6	-0.6
277	20.8	19.3	19.8	4.8	-2.6
291	3.5	3.1	3.1	11.4	0.0
300	-6.9	-6.5	-6.7	2.9	-3.1
311	-20.6	-20.8	-21.1	-2.4	-1.4

CONCLUSIONS

Three-dimensional computational fluid dynamic simulations of a standard 2 × 4, uninsulated 2.44-m (8-ft) tall, wall assembly were performed to evaluate its performance over a wide range of operating conditions. The thermophysical properties of air and wood wall materials were allowed to vary with temperature. Parameters that were varied in this study include the ambient outdoor temperature and cavity surface emissivity. The results can be implemented into building energy simulation tools to improve their accuracy in predicting building energy use in older homes that have uninsulated cavities.

The findings of this study include:

- The variable thermal conductivity of wood products has a significant impact on the assembly's thermal resistance: the assumption of constant thermal conductivity resulted in up to 8% underprediction for colder ambient temperatures (lower thermal conductivity of wood) and 2% overprediction for warmer conditions.
- The variable thermophysical properties of air have no effect on the thermal performance of the wall assembly.
- Three-dimensional flow structures, induced by the wood framing elements, were identified, but they led to minor differences between 3D and 2D predictions of the wall's total resistance. This indicates that a 2D model may be sufficient to predict the thermal resistance of uninsulated wall assemblies.
- In terms of the total heat flux through the wall, 3D and 2D models showed comparable results for winter and summer conditions. Significant differences were found relative to the traditional approach, where the thermal resistance of the assembly is assumed to be constant: 9.3% at 233 K (-40˚F).

The results indicate a potential source of inaccuracy in determining the thermal resistance of uninsulated cavities when the traditional approach is used: at low ambient temperatures, the thermal resistance of wood products may be higher than that evaluated at a fixed temperature.

Future work includes the use of model results to develop correlations that can be used in building energy simulation tools and modifying the model to address air infiltration through the uninsulated assembly. More data on the variable thermal conductivity of wood products are necessary to properly characterize different wood products (siding, sheathing, and stud).

REFERENCES

[1] Bejan, A., 1995, *Convection Heat Transfer*, 2nd ed., Wiley, CA.

[2] Jaluria, Y., 2003, *Natural Convection, in Heat Transfer Handbook*, chap. 7, A. Bejan and A. D. Kraus (eds.), Wiley, New York.

[3] Raithby, G. D., and Hollands, K. G. T., 1998, "Natural Convection," in *Handbook of Heat Transfer*, W. M. Rohsenow et al. (eds.), 3rd ed., McGraw-Hill, New York.

[4] Douamna, S., Hasnaoui, M., and Abourida, B., 2000, "Two-Dimensional Transient Natural Convection in a Repetitive Geometry Submitted to Variable Heating from Below: Numerical Identification of Routes Leading to Chaos," *Numerical Heat Transfer* **A 37**:779-799.

[5] Fusegi, T., Hyun, J.M., Kuwahara, K., 1992, "Natural Convection in a Differentially Heated Square Cavity with Internal Heat Generation," *Numerical Heat Transfer* **A 21**:215-229.

[6] Lakhal, E. K., Hasnaoui, M., Vasseur, P., and Bilgen, E., 1995, "Natural Convection in a Square Enclosure Heated Periodically from Part of the Bottom Wall," *Numerical Heat Transfer* **A 27**:319-333.

[7] Rahman M., and Sharif, M. A. R., 2003, "Numerical Study of Laminar Natural Convection in Inclined Rectangular Enclosures of Various Aspect Ratios," *Numerical Heat Transfer* **A 44**:355-373.

[8] Catton, I., 1978, "Natural Convection in Enclosures," *Proceeding of the Sixth Int. Heat Transfer Conference* **6**:13-32.

[9] Akiyama, M., and Chong, Q. P., 1997, "Numerical Analysis of Natural Convection with Surface Radiation in a Square Enclosure," *Num. Heat Transfer* **A 31:**419-433.

[10] Pak, H. Y., and Park, K. W., 1998. "Numerical Analysis of Natural Convective and Radiative Heat Transfer in an Arbitrarily Shaped Enclosure," *Numerical Heat Transfer* **A 34**:553-569.

[11] Ridouane, E. H, Hasnaoui, M., Amahmid, A., and Raji, A., 2004, "Interaction between Natural Convection and Radiation in a Square Cavity Heated from Below," *Numerical Heat Transfer* **A 45**:289-311.

[12] Yucel, A., Acharya, S., and Williams, M. L., 1989, "Natural Convection and Radiation in a Square Enclosure," *Numerical Heat Transfer* **A 15**:261-278.

[13] Park, J. E., Kirkpatrick, J. R., Tunstall, J. N., and Childs, K. W., 1986, "Calculation of Heat Flux through a Wall Containing a Cavity: Comparison of Several Models," Oak Ridge Gaseous Diffusion Plant, TN, DE86010348.

[14] ASHRAE, 2009, *ASHRAE Fundamentals Handbook*. Atlanta: American Society of Heating Refrigeration and Air-Conditioning Engineers, Inc.

[15] Barbour, E., Goodrow, J., Kosny, J., and Christian, J. E., 1994, "Thermal Performance of Steel-Framed Walls," CRADA Final Report for ORNL93-0235.

[16] Lorente, S., 2002, "Heat Losses through Building Walls with Closed, Open and Deformable Cavities," *International Journal of Energy Research* **26**(7):611-632.

[17] Aviram, D. P., Fried, A. N., and Roberts, J. J., 2001, "Thermal Properties of a Variable Cavity Wall," *Building and Environment* **36**(9): 1057-1072.

[18] Manz, H., 2003, "Numerical Simulation of Heat Transfer by Natural Convection in Cavities of Facade Elements," *Energy and Buildings* **35**(3):305-311.

[19] Xaman, J., Alvarez, G., Lira, L., and Estrada, C., 2005, "Numerical Study of Heat Transfer by Laminar and Turbulent Natural Convection in Tall Cavities of Facade Elements," *Energy and Buildings* **37**(7):787-794.

[20] Antar, M. A., and Baig, H., 2009, "Conjugate Conduction-Natural Convection Heat Transfer in a Hollow Building Block. Applied Thermal Engineering," **29**(17-18):3716-3720.

[21] Ridouane, E. H., and Bianchi, M. V. A., 2011, "Thermal Performance of Uninsulated and Partially Filled Wall Cavities," *Proceedings of the 2011 ASHRAE Annual Meeting*, Montreal, Canada: June 25-29.

[22] Wood Handbook, 2010, W*ood as an Engineering Material*. Centennial Edition, Forest Products Laboratory, U.S. Department of Agriculture Forest Service, Madison, WI.

[23] Modest, M. F., 2003, *Radiative Heat Transfer*, 2nd ed., Academic Press, CA.

[24] FLUENT Inc., 2006, *FLUENT Manual*. Lebanon, NH, FLUENT, Inc.